Nanoscale Advances

ROYAL SOCIETY OF CHEMISTRY

PAPER

View Article Online
View Journal | View Issue

Cite this: *Nanoscale Adv.*, 2021, **3**, 5860

Size-dependent trends in the hydrogen evolution activity and electronic structure of MoS_2 nanotubes†

Charlie Ruffman, J. T. A. Gilmour and Anna L. Garden *

The thermodynamics of hydrogen evolution on MoS_2 nanotubes is studied for the first time using periodic density functional theory calculations to obtain hydrogen adsorption free energies ($\Delta G_{H_{ads}}$) on pristine nanotubes and those with S-vacancy defects. Armchair and zigzag MoS_2 nanotubes of different diameters, ranging from 12 to 22 Å, are examined. The H adsorption energy is observed to become more favourable (lower $\Delta G_{H_{ads}}$) as nanotube diameter decreases, with $\Delta G_{H_{ads}}$ values ranging from 1.82 to 1.39 eV on the pristine nanotubes, and from 0.03 to −0.30 eV at the nanotube S-vacancy defect sites. An ideal thermoneutral $\Delta G_{H_{ads}}$ value of nearly 0 eV is observed at the S-vacancy site on nanotubes around 20 to 22 Å in diameter. For the pristine nanotubes, density of states calculations reveal that electron transfer from S to Mo occurs during H adsorption, and the energy gap between these two states yields a highly reliable linear correlation with $\Delta G_{H_{ads}}$, where a smaller gap leads to a more favourable hydrogen adsorption. For the S-vacancy defect site the H adsorption resembles that on a pure metallic surface, meaning that a traditional d-band centre model can be applied to explain the trends in $\Delta G_{H_{ads}}$. A linear relation between the position of the Mo d-states and $\Delta G_{H_{ads}}$ is found, with d-states closer to the Fermi level leading to strong hydrogen adsorption. Overall this work highlights the relevance of MoS_2 nanotubes as promising hydrogen evolution catalysts and explains trends in their activity using the energies of the electronic states involved in binding hydrogen.

Received 14th June 2021
Accepted 30th August 2021

DOI: 10.1039/d1na00441g

rsc.li/nanoscale-advances

1 Introduction

Molecular H_2 is highly sought after as a carbon-zero energy transport and storage medium,[1–3] as well as a critical reactant in many key industrial processes such as the Haber–Bosch reaction to generate nitrogenous fertilizer.[4] Currently, the majority of H_2 is produced either *via* steam reformation of natural gas or from reformation of fuel oils.[5,6] However, these processes are energy intensive, consume dwindling fossil fuel reserves, and produce harmful by-products such as CO_2.[4] Instead, it is highly desirable to be able to produce large volumes of H_2 through the electrolysis of water, which is a clean process that can be driven by renewable energy sources.[7]

One of the key half-reactions in water electrolysis is the hydrogen evolution reaction (HER), where protons are formally reduced at the cathode ($2H^+ + 2e^- \rightarrow H_2$). Pt and Pt-based catalysts are generally accepted to be the most active for hydrogen evolution,[8–10] yet these materials can be prohibitively expensive on an industrial scale due to the scarcity of Pt. As a result, there has been much attention directed at developing a catalyst for the HER that is competitive with Pt in terms of activity, yet is composed of only Earth-abundant materials. Nanostructured molybdenum disulfide (MoS_2) is one such material, and its promising HER activity has been documented across many studies[11–13] since it was first proposed.[14]

Structurally, bulk MoS_2 is composed of layered 2D sheets, where a single layer constitutes a row of Mo atoms sandwiched between two rows of S atoms. Because the sheets are only held together by weak van der Waals forces, individual layers can be isolated or synthesized as stand-alone structures, which are highly catalytically interesting. In this single-layer form, MoS_2 has a large flat basal plane which both experimental[11] and theoretical evidence[14,15] has indicated is inactive to hydrogen evolution. However, MoS_2 catalysts also have exposed edges that dominate the reactivity,[11,16] despite making up a relatively small proportion of the material.

Unfortunately, the activity of most MoS_2 catalysts falls short of the current standard, Pt, by around two orders of magnitude.[11,13,17] However, there is also substantial room to improve the performance of MoS_2. A very large body of work has been devoted to improving the HER on the edges of MoS_2 through heteroatom doping with Co[18] or Ni,[19] or supporting the thin MoS_2 on other materials which modify its activity.[16,20,21] Because the HER activity of the MoS_2 edges is already high, another

MacDiarmid Institute for Advanced Materials and Nanotechnology, Department of Chemistry, University of Otago, P.O. Box 56, Dunedin 9054, New Zealand. E-mail: anna.garden@otago.ac.nz

† Electronic supplementary information (ESI) available. See DOI: 10.1039/d1na00441g

promising way in which the overall catalyst could be improved is by activating the basal plane, as this inert portion actually makes up the majority of the catalyst. The present work focuses on this latter approach.

A large contributor to the poor HER activity on the MoS_2 basal plane is that the thermodynamics of the reaction are highly unfavourable.[14] Because the HER is a two-step process where H must first adsorb to the catalyst then two H atoms combine to form H_2, the energy of the intermediate H_{ads} state fully captures the thermodynamics of the overall reaction. Following the Sabatier principle,[22] the catalyst should not bind H so strongly that it requires large amounts of energy to desorb and form H_2 ($\Delta G_{H_{ads}} \ll 0$), nor so weakly that it is difficult to get H adsorbed in the first place (*i.e.* $\Delta G_{H_{ads}} \gg 0$). The thermodynamically optimal catalyst has $\Delta G_{H_{ads}} = 0$. It is known the pristine basal plane of MoS_2 binds H too weakly ($\Delta G_{H_{ads}} > 2.0$ eV)[21] to facilitate hydrogen evolution. This contrasts to the much more favourable $\Delta G_{H_{ads}}$ value of -0.30 eV on the MoS_2 edge,[21] and the even more favourable -0.03 eV on Pt(111) under electrocatalytic conditions.[17] In the past, $\Delta G_{H_{ads}}$ on the basal plane has been brought closer to thermoneutral (0 eV) by addition of conducting graphene derivative supports,[21,23] doping with heteroatoms,[24,25] creation of S-vacancy defects,[26] or laterally straining the MoS_2 sheet.[27] Often, these techniques can be used in conjunction with each other to produce promising results, though they can be synthetically complex and require precision. Additionally, multiple high-resolution transmission electron microscopy studies have suggested that S vacancy defects are common in the basal plane of MoS_2,[28] with site densities of up to 10^{13} per cm^2.[29] DFT studies also confirm the likelihood of S-vacancies in the basal plane,[26,30,31] finding that they affect both the electronic properties of the basal plane and significantly lower the H adsorption energy.[31]

Another way to activate the basal plane is to use a structural form of MoS_2 that has a lower $\Delta G_{H_{ads}}$ and higher intrinsic activity. Perhaps the most well known of these is 1T-MoS_2, where an artificially induced phase-transition causes a shift to metallic behaviour on the basal plane.[32,33] However, recently, several experimental studies have reported high HER activity from nanotube structures formed out of single-layer 2H-MoS_2,[34–36] where the layer of MoS_2 is coiled up analogous to how carbon nanotubes are formed by rolling graphene. The nanotube form of MoS_2 is relatively easy to synthesise, either with a single wall, multiple walls, or with a core material.[37,38] The enhanced catalytic activity of the nanotubes compared to flat structures suggests that the strain placed on the basal plane by rolling it into a tube may somehow activate it to adsorbing H. This is reasonable to expect, as Shi *et al.*[39] have previously shown that mechanical bending of flat forms of MoS_2 can strengthen the H adsorption energy. Furthermore, the electronic structure in MoS_2 nanotubes is known to change compared to flat structures, showing smaller band gaps[40,41] and enhanced charge carrier mobility,[42] both of which are features that are associated with high catalytic activity. Very recently, Cardoso *et al.*[43] were able to show that electronic structure changes in nanotubes of different diachalcogenides, WS_2 and WSe_2, were responsible for improved H adsorption energies, and thus better HER performance. Therefore, it is of great interest to understand how the electronic structure in MoS_2 nanotubes differs from that of the flat basal plane, and whether this can be related to the HER performance.

In addition to being different from the flat basal plane, it has long been established that the surface and electronic properties of MoS_2 nanotubes are highly size dependent. Seifert *et al.*[44] show that the strain energy of small MoS_2 nanotubes (between 8 and 26 Å in diameter) increases notably as tubes get smaller. At the same time, the smaller nanotubes begin to behave more like conducting materials instead of semiconductors. More recently, Ansari *et al.*[45] reported a near-linear decrease in the band gap of MoS_2 nanotubes as the diameter decreased. If this relation is extrapolated, the band gap would approach 0 eV (*i.e.* conducting) at around 10 Å in diameter. In studying charge carrier mobility, Xiao *et al.*[42] report notable deferences between the electron and hole mobility for two different ways of coiling MoS_2 nanotubes: armchair and zigzag. The authors also see that the carrier mobility changes notably with the size of the nanotube. Given that altered electronic conductivity and a reduction of the band gap could be critical to HER catalysis,[21] in the present work we study how the H adsorption free energy shifts between different sized nanotubes, for both armchair and zigzag structures. It can also be determined whether any observed effects on $\Delta G_{H_{ads}}$ can be underpinned by the electronic structure changes.

Density functional theory calculations of $\Delta G_{H_{ads}}$ on MoS_2 nanotubes are used to explore the activation of the basal plane by reducing the thermodynamic cost to adsorbing or desorbing H. Armchair and zigzag nanotubes of diameters varying from 12 to 22 Å are studied, and both pristine and S-vacancy defect sites are considered. We find a reliable tendency for H adsorption to become more favourable as nanotube diameter decreases, regardless of adsorption site. Density of states calculations are used to rationalise this trend in terms of the energetic position of the S p-states and Mo d-states involved in binding H.

2 Methodology

2.1 Structure models

The flat basal plane of MoS_2 was simulated using a single-layer slab, periodic in two dimensions, with an explicit unit cell measuring 5×5 Mo atoms. It was calculated to have a lattice constant of 3.18 Å, representing spacing between Mo atoms. At least 12 Å of vacuum separation was ensured between repeats in the non-periodic direction, perpendicular to the basal plane.

To form MoS_2 nanotubes, an extended sheet of flat single-layer MoS_2 was coiled about a chiral vector, $\overrightarrow{Ch}$, as seen in Fig. 1A. In this case, the shaded region makes up the atoms in the nanotube, and the two grey ends will meet when coiled. $\overrightarrow{Ch}$ runs along the circumference of the coiled nanotube. The length and direction of $\overrightarrow{Ch}$ comes from the sum of two vectors, $\vec{n}$ and $\vec{m}$ which are at 60° to each other. Coiled nanotubes are described by the length of their $\vec{n}$ and $\vec{m}$ vectors in terms of the number of primitive cell repeats $(\vec{n}, \vec{m})$. The example in Fig. 1A is a (3, 3) tube, which is smaller than is realistic and is included for illustration purposes only. Armchair nanotubes are defined by $\vec{n}$ and $\vec{m}$ having the same length, whereas for zigzag nanotubes

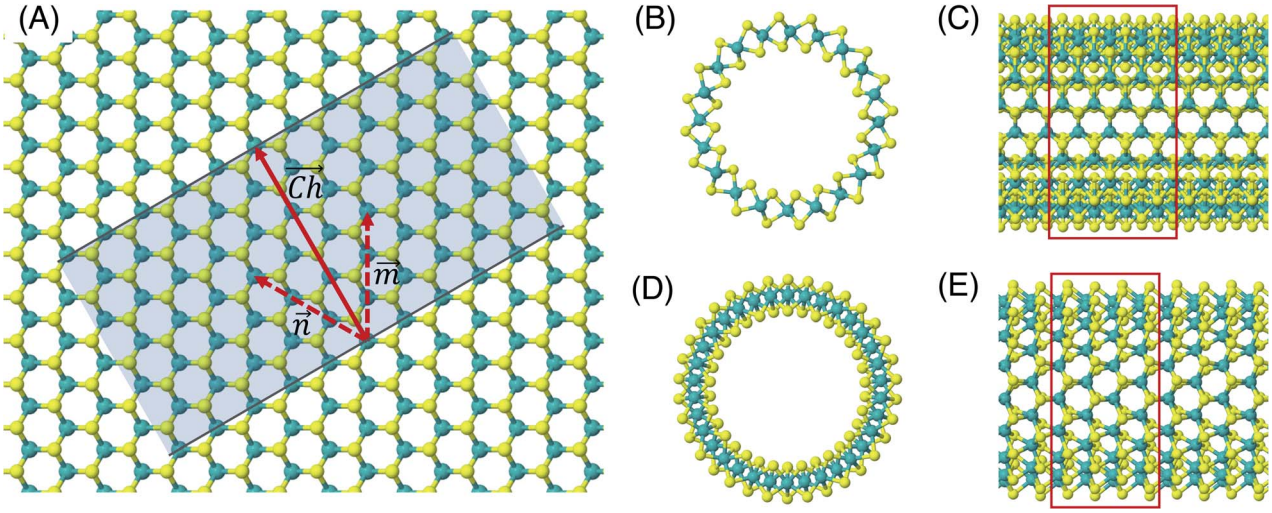

Fig. 1 (A) A schematic showing how MoS_2 nanotubes are related to the flat basal plane. The shaded area indicates the nanotube that could be rolled along chiral vector, $\overrightarrow{Ch}$, so that the two darker edges meet. The sum of the $\vec{n}$ and $\vec{m}$ vectors define the length and direction of $\overrightarrow{Ch}$, here giving a (3, 3) armchair nanotube. The (B) end-on and (C) side views of a (10, 10) armchair nanotube. The (D) end-on and (E) side views of a (17, 0) zigzag nanotube. Note that these two examples both have approximately the same internal diameter. The red boxes give and indication of the unit cell in the periodic direction, but the heights of these boxes are not to scale.

the $\vec{m}$ vector is always zero and $\vec{n}$ can have any value. Examples of realistic coiled armchair and zigzag nanotubes are also given in Fig. 1.

In a computational representation of the nanotubes, there is one periodic direction along the length of the tube and two non-periodic directions. The explicitly simulated repeating cell in the periodic direction was 4 units long, as shown in Fig. 1C and E. At least 12 Å of vacuum spacing was ensured in the non-periodic directions either side of the nanotube.

2.2 Computational details

The structures were relaxed and electronic energies calculated using periodic density functional theory (DFT), as implemented in the Vienna ab initio simulation package (VASP).[46] The form of the electron density, and thus the energy, was obtained *via* iterative diagonalization of the Kohn–Sham Hamiltonian. A Bayesian error estimation exchange–correlation functional with the inclusion of van der Waals forces (BEEF-vdW),[47] was chosen, which represents the generalised gradient approximation level of theory. This functional is optimised for studying surface catalytic processes, making it an ideal fit here. A periodic plane-wave basis set with a kinetic energy cut-off of 500 eV was used to describe the valence electrons, whereas core electrons were described using the projector augmented wave method.[48,49] To aid convergence, the energetic states of valence electrons were smeared according to a Fermi–Dirac distribution where $k_BT = 0.1$ eV. For density of states calculations, the smearing width was reduced to 0.01 eV in order to provide finer resolution of the states. All reported energies were extrapolated to $k_BT = 0$. When relaxing geometries, the coordinates of nuclear centres were updated in the direction of the forces acting on them until the total force on each centre was less than 0.03 eV $Å^{-1}$. For the flat basal plane, reciprocal space was sampled using 4 × 4 × 1 Monkhorst–Pack *k*-point scheme. For nanotubes, where only one dimension is periodic, a 4 × 1 × 1 scheme was used instead.

The strain on nanotube models due to their curvature, ΔE_{strain}, was calculated per Mo atom relative to a flat surface of the same size, following established methodology:[50]

$$\Delta E_{strain} = \frac{E_{tube} - E_{flat}}{n_{Mo}} \quad (1)$$

where E_{tube} is the electronic energy of the pristine nanotube, E_{tube} is the energy of an equivalent flat MoS_2 surface, and n_{Mo} is the number of Mo atoms in a model.

The formation energies (ΔE_f) of each of the different nanotube structures were computed relative to bulk Mo and S in H_2S:

$$\Delta E_f = \frac{E_{tube} - N\left(E_{Mo,ref} + 2E_{S,ref}\right)}{N} \quad (2)$$

where N is the number of MoS_2 units, $E_{Mo,ref}$ is the energy of a single Mo atom in the body centred cubic bulk, and $E_{S,ref} = E_{H_2S} - E_{H_2}$. A more rigorous analysis using the chemical potentials of S and Mo can be performed,[51] but this is unnecessary for simply comparing trends between similar systems. The electronic energy of the H_2S reference system has been employed successfully in previous work.[52]

The formation energies of S-vacancy defects ($\Delta E_{f,vac}$) were also computed as:

$$\Delta E_{f,vac} = E_{tube+vac} + E_{S,ref} - E_{tube} \quad (3)$$

Electronic H adsorption energies ($\Delta E_{H_{ads}}$) were calculated *via* eqn (4):

$$\Delta E_{H_{ads}} = E_{MoS_2} + H - \left(E_{MoS_2} + \frac{1}{2}E_{H_2}\right) \quad (4)$$

where E_{MoS_2} + H is the energy of the MoS_2 structure (nanotube or flat basal plane) with H adsorbed, E_{MoS_2} is the energy of only the MoS_2 structure, and $\frac{1}{2}E_{H_2}$ is half the energy of H_2 in a vacuum. Electronic adsorption energies were converted to Gibbs free energies as shown in eqn (5):

$$\Delta G_{H_{ads}} = \Delta E_{H_{ads}} + \Delta(\mathrm{ZPE}) - T\Delta S \quad (5)$$

where Δ(ZPE) and $T\Delta S$ are the differences in the zero point energy and entropy relative to gas phase hydrogen and are obtained through normal mode analysis. The value of the [Δ(ZPE) − $T\Delta S$] contribution in eqn (5) was tested across multiple different adsorption sites. On the flat basal plane, this was found to be consistently around 0.23 eV regardless of the site H adsorbed to. On the MoS_2 nanotubes, the value was slightly higher at 0.25 eV, and it did not depend on nanotube size. For adsorbing H to S-vacancy sites, [Δ(ZPE) − $T\Delta S$] was lower at 0.21 eV on both the basal plane and nanotubes.

3 Results and discussion

3.1 Pristine MoS_2 nanotubes

The optimised values for the lattice constant (in the periodic direction along the axis of the nanotube) and the diameter of the different armchair and zigzag nanotubes tested here are presented in Table 1. For the all the different sized armchair nanotubes, the lattice constant of the 1D tube in the periodic direction is very slightly longer than that for the flat basal plane of MoS_2 (3.18 Å). In contrast, for the zigzag nanotubes, this lattice constant is shorter than the basal plane. These patterns are highly consistent with past results.[41] When moving to larger sizes, the lattice constant for both types of nanotube appears to trend in the direction of the bulk value.

In terms of the nanotube internal diameters, a reasonable range is able to be simulated for both armchair and zigzag nanotubes, spanning in total from 11.91 Å to 21.88 Å. While most of the sizes reported here are smaller than those that are typically observed in experiment,[38] the largest of the MoS_2 nanotubes crosses over with the size of some of the smaller cases observed experimentally.[53] The diameter range we report is similar to that of other DFT works.[42,44]

The strain energy due to curvature (calculated *via* eqn (1)) is also presented in Table 1. There is a consistent trend for strain to increase as the nanotube diameter, d, gets smaller. Plots in the ESI (Fig. S1†) show that the strain appears to follow a $\frac{1}{d^2}$ relation with nanotube diameter, which was originally reported by Seifert *et al.*[44] Some of the smallest nanotubes studied here can be considered highly strained, with an energy difference of 0.73 eV per Mo atom compared to the flat surface. The strain effects are also clearly reflected in the formation energies of the nanotubes. While all of the materials studied here are stable relative to their constituent atoms, the flat basal plane has the most favourable formation energy, and the formation energy becomes less negative as the nanotubes get smaller. There is no notable difference between ΔE_f for armchair and zigzag nanotubes.

On the MoS_2 basal plane, three stable H adsorption sites are located: directly on top of an S atom (Fig. 2A, $\Delta G_{H_{ads}} = 2.24$ eV), in a tilted configuration on an S atom at approximately 40° from the upright (Fig. 2B, $\Delta G_{H_{ads}} = 2.04$ eV), and directly on an Mo atom ($\Delta G_{H_{ads}} = 2.79$ eV). Each of these H adsorption sites was

Table 1 Optimised geometric parameters of the pristine nanotubes studied in the present work. The lattice constant is measured in the periodic direction along the axis of the nanotube, and the diameter is measured internally from two S atoms on the inside of the tube. Also shown are the formation energies, the strain energy per circumference Mo (relative to a flat surface of the same size), ΔE_{strain}, and the free energy of H adsorption, $\Delta G_{H_{ads}}$, at both an S and Mo site on the outside of the nanotubes

System ($\vec{n}$, $\vec{m}$)	Lattice constant/Å	Diameter/Å	ΔE_f/eV	ΔE_{strain} per Mo/eV	$\Delta G_{H_{ads}}$ S/eV	$\Delta G_{H_{ads}}$ Mo/eV
Basal plane						
	3.18	—	−2.22	—	2.24	2.79
Armchair						
(8, 8)	3.21	11.91	−1.49	0.73	1.39	1.55
(9, 9)	3.21	13.56	−1.63	0.59	1.51	1.70
(10, 10)	3.21	15.16	−1.73	0.49	1.60	1.83
(11, 11)	3.20	16.75	−1.81	0.41	1.67	1.91
(12, 12)	3.20	18.60	−1.87	0.34	1.74	2.01
(13, 13)	3.20	20.36	−1.92	0.30	1.79	2.11
(14, 14)	3.20	22.08	−1.96	0.26	1.82	2.13
Zigzag						
(14, 0)	3.14	12.26	−1.52	0.69	1.44	1.52
(15, 0)	3.14	13.16	−1.60	0.61	1.52	1.67
(17, 0)	3.16	15.00	−1.73	0.49	1.60	1.80
(19, 0)	3.16	16.96	−1.82	0.40	1.70	1.88
(20, 0)	3.17	17.91	−1.86	0.36	1.72	1.90
(22, 0)	3.17	19.97	−1.91	0.30	1.79	2.06
(24, 0)	3.17	21.88	−1.96	0.26	1.82	2.06

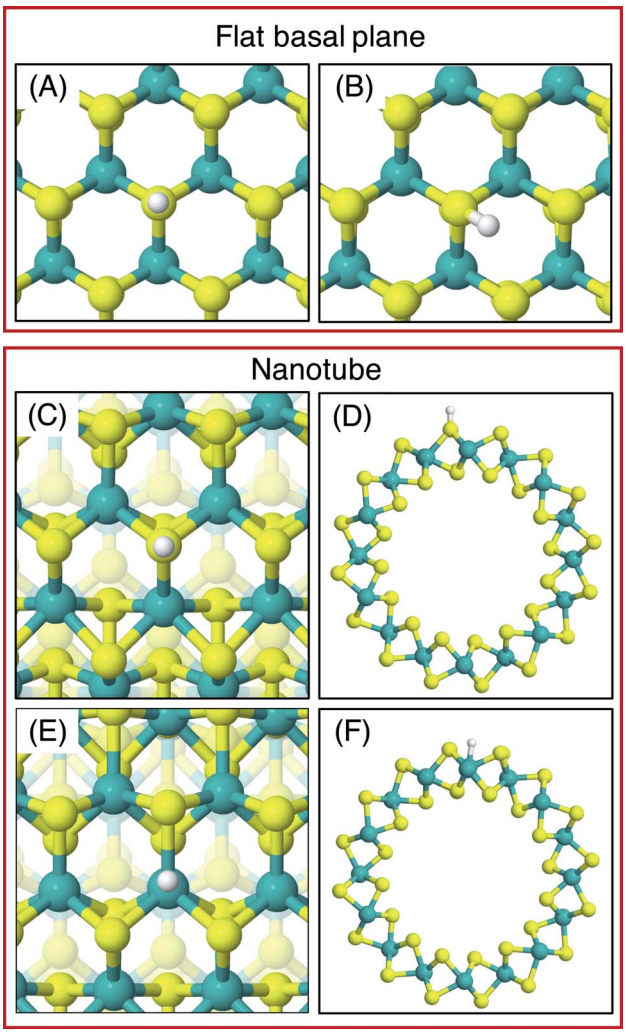

Fig. 2 Favourable adsorption site geometries on the basal plane and on the outside of an armchair nanotube. (A) shows the on-top S site and (B) shows the tilted S site, both on the basal plane. (C) and (D) show top and side views of H adsorption to an outside S on the armchair nanotube, and (E) and (F) show the same for Mo adsorption. These geometries are also representative of H adsorption on the zigzag nanotubes.

tested on the MoS_2 nanotubes. However, the tilted H configuration could not be located on nanotubes of any size tested here, despite it being preferable on the flat MoS_2 basal plane.[54] Locating the titled geometry has been difficult in past works on flat MoS_2 also, where supports beneath the catalyst prevented it being found.[21] It is suggested that this tilted configuration is highly sensitive to perturbations of the MoS_2 structure, and thus we proceed only with the stably located S on-top and Mo sites for the nanotubes. The H adsorption energy at the S site on the flat basal plane is 0.1–0.2 eV higher than some previous estimates,[15] which is likely accounted for by the finer *k*-point mesh and larger model size employed here.

Unlike the basal plane which has symmetric faces, the sites inside and outside of the MoS_2 nanotubes are inequivalent. To compare inside and outside H adsorption, three sizes for each of armchair and zigzag nanotubes were chosen as a representation of different diameters: (8, 8), (11, 11) and (14, 14) for armchair, and (14, 0), (19, 0) and (24, 0) for zigzag. The raw electronic adsorption energies for the inside and outside sites on these structures are available in the ESI (Table S1†). The overall trends indicated a strong and reliable preference for H adsorption on the outside of the nanotube as opposed to the inside, by on average 0.30 eV for S sites and 0.85 eV on Mo sites. The geometries of these favourable outside binding sites are pictured for an armchair nanotube in Fig. 2 at the S site (C and D) and the Mo site (E and F).

One possible reason for the preference to adsorb on the outside of the nanotube is a small but reliable charge disparity between the S atoms on the outside of the tube and those on the inside. Bader charge analyses of these centres in (8, 8) armchair MoS_2 indicated the average net charge on the outside S atoms was $-0.68e^-$, and for the inside S atoms was $-0.57e^-$. This is in contrast to the flat basal plane, where the average Bader charge on the S atoms lies somewhere between these two values, at $0.61e^-$. A similar pattern was observed for larger nanotubes and also the zigzag nanotubes (see Fig. S2 to S7 in the ESI†). Considering the fairly large number of atoms this charge differential is distributed over, this indicates a reliable preference for electron density to be on the outside of the nanotube.

The $\Delta G_{H_{ads}}$ values for the S and Mo sites on the outside of all nanotubes studied here are presented in Table 1, and these values are plotted against the nanotube diameter in Fig. 3A. There is a clear preference for adsorption at the S site over the Mo at the largest nanotube sizes by 0.31 eV on the armchair nanotubes and 0.24 eV on the zigzag nanotubes, but this difference in energy drops to only 0.16 eV and 0.08 eV, respectively, at the smallest sizes (clearly observed in Fig. 3A). For all nanotubes, this difference is significantly smaller than the 0.55 eV on the flat basal plane, suggesting that the S and Mo sites are far more competitive on nanotubes, especially those with small diameters. This may have mechanistic ramifications, as H diffusion to an Mo atom has previously been implicated as an important step in the HER on MoS_2 edge structures,[55,56] though this has not yet been explored on the basal plane of 2H-MoS_2.[57]

Examining how $\Delta G_{H_{ads}}$ changes with the diameter of different nanotubes, there is a clear trend for H adsorption to become more favourable as the nanotubes get smaller (Fig. 3A). Interestingly, no notable difference in $\Delta G_{H_{ads}}$ between armchair and zigzag nanotube structures is observed, other than that induced by their slightly different diameters. This suggests that the local electronic and geometric structure around the H adsorption site is the same for both classes of nanotube. The most favourable adsorption energy found here is 1.39 eV, reported at an S atom site on the (8, 8) armchair nanotube with a diameter of slightly less than 12 Å. This is significantly lower than the 2.24 eV adsorption energy on the flat basal plane of MoS_2, suggesting the nanotubes likely have enhanced HER activity, yet still is significantly higher than thermodynamically ideal. This finding can be partly explained by smaller nanotubes having higher strain energies. In Fig. 3B, it can be seen that the $\Delta G_{H_{ads}}$ relates very closely to ΔE_{strain}. This linear relation may be highly useful for predicting $\Delta G_{H_{ads}}$ values on different sized

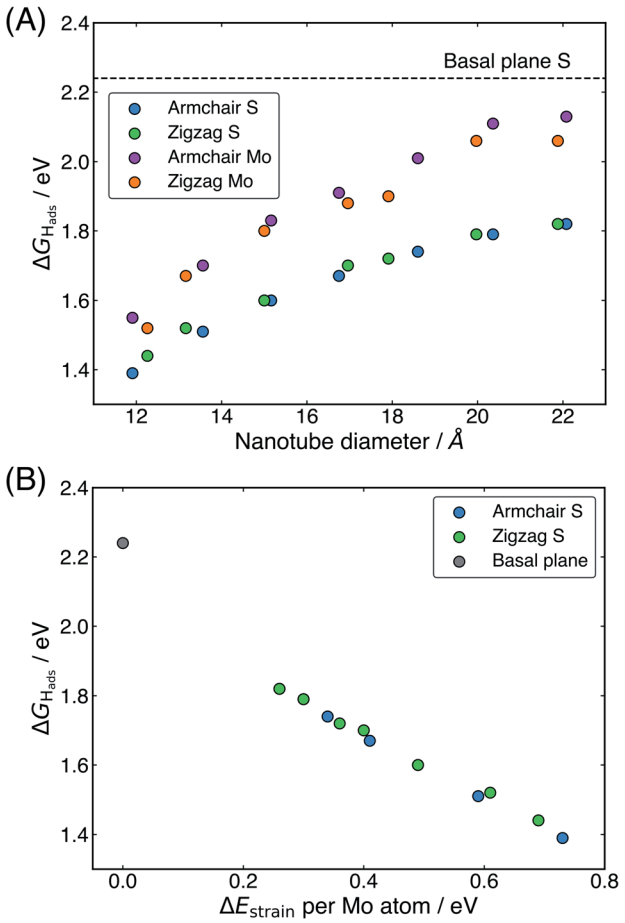

Fig. 3 (A) The hydrogen adsorption free energy, $\Delta G_{H_{ads}}$, as a function of diameter for both armchair and zigzag nanotubes. (B) The linear relation between strain energy (ΔE_{strain}) and $\Delta G_{H_{ads}}$. Note that it may appear there are fewer armchair nanotube data points than zigzag, but this is because several values fall in exactly the same place on the plot. For both plots, $\Delta G_{H_{ads}}$ on the flat basal plane S site is also shown for comparison.

nanotubes, or even curved MoS_2 surfaces. However, while it makes sense intuitively that higher strained materials may bind H stronger, it remains unclear what electronic and bonding factors underpin this behaviour. This point will be revisited and addressed in Section 3.3 later.

One interesting question is to what extent the present relation between $\Delta G_{H_{ads}}$ and nanotube diameter or strain can be extrapolated. For instance, it is possible that $\Delta G_{H_{ads}}$ values closer to 0 eV could be reached going to nanotubes smaller than 12 Å in diameter, corresponding to higher strain energies. When this idea was tested here, it was found these nanotubes were highly unstable, and tended to distort and break apart when H was adsorbed to the system. The breaking apart of the nanotubes is not overly surprising, given these particularly small systems would be under relatively high strain. This suggests that 12 Å diameter may pose a lower limit on the size of MoS_2 nanotubes for surface catalysis applications at least. Looking at the larger sizes of nanotubes, it is possible that the relation could be extrapolated to a nanotube of infinite diameter, which should in theory match the $\Delta G_{H_{ads}}$ of the basal plane. However, without additional testing of H adsorption on nanotubes larger than the maximum size reported here, making this extrapolation is difficult as it is unclear whether the relation between diameter and $\Delta G_{H_{ads}}$ is linear in nature or curvilinear, in which case it may asymptote. Unfortunately larger sizes were outside the scope of the DFT calculations able to be performed here. Though, it is possible future work could be done using a limited selection of larger nanotubes or models that had fewer repeats in the periodic direction of the tube.

3.2 S-vacancy defects in MoS_2 nanotubes

Given that even the smallest MoS_2 nanotubes obtainable here still produced $\Delta G_{H_{ads}}$ values that were much higher than the desired thermoneutral 0 eV, this alone was unlikely to be able to explain the experimentally observed enhanced catalytic activity of the nanotubes relative to the basal plane.[35,58,59] Therefore, nanotubes with S-vacancy defects were also investigated. Previous reports on defects in MoS_2 nanotubes report S-vacancies modifying the mechanical[60] and electronic or magnetic properties,[61] but the H adsorption energy has yet to be explored. Here, single S-vacancies are studied, where one S atom is removed from the outside of the nanotube. This was done for each of the sizes of pristine nanotube tested in the previous section. No notable structural distortion was observed on relaxation after a defect had been created. The vacancy formation energies (Table 2) indicate that it is about 0.3 eV more favourable for an S-vacancy to form on the flat basal plane than on the nanotube structures, which is likely a result of the added strain in the nanotube. However, there is very little variance observed between different nanotube sizes, and the vacancy formation energies are not prohibitively large.

Table 2 Vacancy formation energies, $\Delta E_{f,vac}$, and H adsorption free energies, $\Delta G_{H_{ads}}$, at S-vacancy defect sites on MoS_2 nanotubes

System ($\vec{n}$, $\vec{m}$)	$\Delta E_{f,vac}$/ eV	$\Delta G_{H_{ads}}$ S-vacancy/eV
Basal plane		
	2.49	0.15
Armchair		
(8, 8)	2.74	−0.30
(9, 9)	2.80	−0.22
(10, 10)	2.82	−0.16
(11, 11)	2.81	−0.13
(12, 12)	2.82	−0.08
(13, 13)	2.81	−0.05
(14, 14)	2.81	−0.05
Zigzag		
(14, 0)	2.79	−0.12
(15, 0)	2.80	−0.10
(17, 0)	2.82	−0.05
(19, 0)	2.82	−0.02
(20, 0)	2.84	−0.01
(22, 0)	2.82	0.01
(24, 0)	2.77	0.03

As was done for the pristine nanotubes, different H adsorption sites were investigated. On the flat basal plane with an S-vacancy, the most favourable adsorption site was found to be at the centre of the three Mo atoms directly below where the S has been removed (Fig. 4A), which is consistent with past work.[31] This position is at least 0.5 eV more favourable than when H is situated on the S atoms surrounding the defect, and if H was positioned directly on top of one of the Mo atoms at the S-vacancy, it always relaxed such that it was centred between all three Mo. Interestingly, this was not the most favourable site on the defective MoS_2 nanotubes – here H instead preferred to adsorb at a bridged position between only two of the Mo atoms underneath the S-vacancy for both armchair and zigzag nanotubes (Fig. 4B and C).

The different adsorption site preference for nanotubes is likely the result of inequivalent Mo atoms in the triangle below the S-vacancy defect. Because of the strain induced by coiling into a tube, two sides of the triangle of Mo atoms have longer bond lengths than the other. In the (8, 8) armchair nanotube the long Mo–Mo bonds are 3.47 Å and the short bond is 3.15 Å. For the (14, 0) zigzag nanotube, there is one long bond of 3.53 Å and two short bonds of 3.23 Å. H adsorbing in the bridged position at any of the short Mo–Mo bonds is the preferred site. Indeed, a stable adsorption geometry in the long bond position could not be located, and instead H would always diffuse to the short Mo–Mo bond site during relaxation.

The $\Delta G_{H_{ads}}$ values for adsorption at the S-vacancy sites across all the nanotubes tested here are reported in Table 2. A substantial drop in $\Delta G_{H_{ads}}$ compared to the pristine surfaces (Table 1) is observed both on the flat basal plane, and across all nanotubes. First looking at the flat basal plane, the $\Delta G_{H_{ads}}$ of 0.15 eV is much closer to thermoneutral than for the pristine surface, a finding which is in close agreement with past work[26] and indicates that the S-vacancy site is far more likely to be active for hydrogen evolution. For the nanotube structures, where the curvature was already seen to decrease $\Delta G_{H_{ads}}$ relative to the flat basal plane for pristine systems, $\Delta G_{H_{ads}}$ values at the S-vacancy site are also lowered and are actually negative for many of the sizes tested here. The negative values indicate that some nanotube S-vacancies actually bind H too strongly to be thermodynamically ideal, in stark contrast to the very weak H binding on the pristine flat basal plane of MoS_2.

Examining the effect of nanotube diameter on $\Delta G_{H_{ads}}$ for the S-vacancy sites (Fig. 5), it is clear that there is still a degree of tuning with size. However, compared to the pristine nanotubes, where the $\Delta G_{H_{ads}}$ on S spanned a total 0.43 eV across diameters from approximately 12 to 22 Å, here the $\Delta G_{H_{ads}}$ only varies by 0.25 eV for armchair and 0.15 eV for zigzag nanotubes across the same range. Interestingly, the range of $\Delta G_{H_{ads}}$ values that are produced with different diameters spans the thermodynamically ideal region around 0 eV. These data suggest that nanotubes around the size of 17–22 Å in diameter would have S-vacancies with near ideal $\Delta G_{H_{ads}}$ values for hydrogen evolution. Given that it is well known that specific active sites can dominate the activity of a catalyst even if they are not overly abundant,[62,63] these S-vacancy sites could easily explain the high HER activity observed on experimentally synthesised MoS_2 nanotubes. An interesting topic for further study would be to explore $\Delta G_{H_{ads}}$ values as the nanotubes get larger than 22 Å in diameter. The trend observed here suggests $\Delta G_{H_{ads}}$ could remain close to 0 eV at these larger diameters.

From Fig. 5 it is also clear that H adsorbing to armchair nanotube S-vacancies is consistently more favourable than the same site on zigzag nanotubes. This contrasts to the pristine structures, where armchair and zigzag tubes produced very similar $\Delta G_{H_{ads}}$ values. This difference is likely a result of different Mo–Mo bond lengths at the bridged H adsorption site on the S-vacancy. As mentioned earlier, the Mo–Mo bonds are slightly shorter for the armchair nanotube (3.15 Å) than the

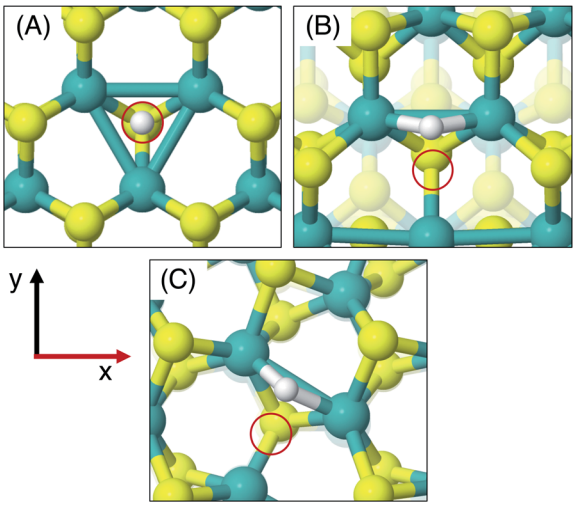

Fig. 4 Geometries of the most favourable H adsorption sites for systems with an S-vacancy defect. (A) shows the flat basal plane, (B) the armchair nanotube, and (C) the zigzag nanotube. Note the preferred adsorption at a bridged position between Mo atoms for the nanotube cases compared to the threefold site for the flat basal plane. In all cases the red circles indicate the position of the S atom removed to create the vacancy.

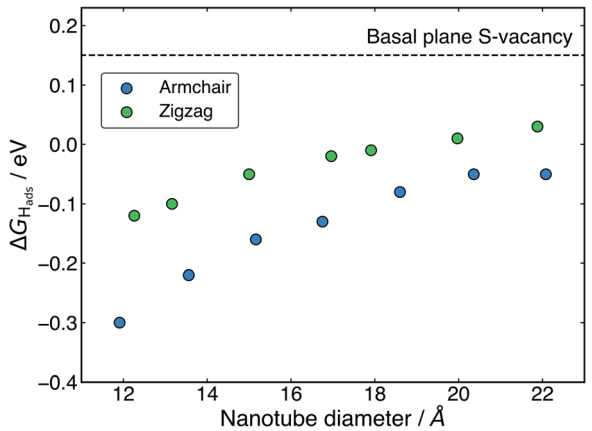

Fig. 5 The hydrogen adsorption free energy, $\Delta G_{H_{ads}}$, at the S-vacancy defect as a function of diameter for both armchair and zigzag nanotubes. $\Delta G_{H_{ads}}$ on the flat basal plane S-vacancy site is also shown for comparison.

zigzag (3.23 Å). This fits with the idea that it is more favourable for H to bind at short Mo–Mo bonds. As a result, while zigzag nanotubes span the ideal thermoneutral range between 17 and 22 Å in diameter, the armchair nanotubes still bind H slightly too strongly in this same diameter range. Indeed, it seems that slightly larger armchair nanotubes may be ideal, where these larger tubes are perhaps easier to obtain experimentally.[38]

3.3 Explaining the trends in H adsorption

In order to better understand what factors might be underpinning the changes in $\Delta G_{H_{ads}}$ observed with different nanotube diameters, investigations into the electronic structure were performed. In this section we consider only the most favourable H binding sites, which for the pristine nanotubes is on an S atom, and for the defective nanotubes is at a bridged position between Mo. Density of states (DOS) calculations were performed for all the clean and H adsorbed nanotubes studied here, including the S-vacancy defect systems and the basal plane. Furthermore, the charge movement arising from H adsorption was explored using Bader charge analyses. The results from these calculations are discussed in the following sections, separately for the pristine MoS_2 systems and the S-vacancy systems.

3.3.1 Pristine basal plane. DOS plots for the atoms around the H adsorption site on the basal plane, smallest and largest armchair nanotubes, and the smallest and largest zigzag nanotubes are all presented in Fig. 6. DOS plots are shown for the system with and without H adsorbed, allowing us to observe the electronic structure change after H binds to the surface. The same DOS analyses were performed for all sizes of nanotubes studied here, and the plots are available in the ESI.†

For the flat basal plane of MoS_2 (Fig. 6A and B), when H adsorbs directly on-top of an S atom a sharp low-energy state with H s and S p character arises, indicating a S–H covalent bond has formed. Additionally, in the H_{ads} system, a new feature arises at the Fermi level primarily composed of partially filled Mo d-states, suggesting the Mo d orbitals are also involved in bonding. This is highly consistent with Liu *et al.*'s recent model for H binding on MoS_2 surfaces,[54] where it is argued that S in the flat MoS_2 basal plane has a full valence and must displace an electron to a neighbouring atom to form a bond with H. Here we suggest some of the S atom's electron density becomes shared across neighbouring Mo atoms. This idea is also supported by the Bader charge analyses of the clean and H_{ads} systems, which show that S loses about 0.2 electron-equivalents of charge and the surrounding Mo atoms together gain around $0.1e^-$.

When H adsorbs to the MoS_2 nanotubes, a very similar pattern of S–H bond formation and electron displacement to Mo is observed. Additionally, the same pattern of charge movement from S to Mo is also observed, and this remains at the same magnitude as the basal plane for all armchair nanotubes tested here (Table S2 in the ESI†). This indicates that the mode of H binding is likely the same as on the flat basal plane. However there are notable differences in the DOS between nanotubes of different sizes. Specifically, in the clean nanotube DOS, it appears that the gap between the edge of the filled S p-states and the unfilled Mo d-states reduces in smaller nanotubes. It has previously been found that the overall band gap of MoS_2 nanotubes reduces with their diameter,[42,45] but here the S p- and Mo-d states are studied specifically, because H binding involves an electron transfer between these two states. We propose that the lowering of $\Delta G_{H_{ads}}$ values on smaller nanotubes is a direct result of the reduction of this energy gap. Indeed, a very reliable linear correlation can be drawn between $\Delta G_{H_{ads}}$ and the energy gap between filled S p- and unfilled Mo d-states (Fig. 7). Extrapolating the linear trend suggests that, as the energy gap approaches zero, the $\Delta G_{H_{ads}}$ value will fall to ~0.8 eV, at which point the energy cost to adsorbing H may predominantly relate to the relaxation and movement of the nuclei.[30] The flat basal plane of MoS_2 is also included in Fig. 7, and lies closely on the trend described by nanotubes of different diameter. This is further evidence that the mode of H binding is the same.

Interestingly, a linear relation was not observed when $\Delta G_{H_{ads}}$ was plotted against the energy of the S p-state edge on its own (see ESI Fig. S8†), suggesting it is specifically the electron transfer from S to Mo that is responsible for part of the energy cost to adsorbing H. This demonstrates that, while the p-state energy may play a role in determining $\Delta G_{H_{ads}}$, it is only considering the difference in energy between the S p- and Mo d-states (*i.e.* those directly involved in electron rearrangement on H adsorption) that yields a direct correlation to $\Delta G_{H_{ads}}$.

3.3.2 S-vacancy defect site. In the case of H adsorbing to the S-vacancy site, the much more favourable $\Delta G_{H_{ads}}$ values indicate that this binding is likely governed by different factors than for the pristine MoS_2 surfaces. Indeed, in looking at the DOS plots for the defective flat basal plane (Fig. 8A and B), it is clear that there is no distinct covalent bond between H and the surface like there is when H is bonded to an S site on the pristine surface. Instead, the H s-state density appears to overlap with both S p- and Mo d-state density across a wider region. This broad region is more pronounced for the nanotube cases which are also presented in Fig. 8. Rather than the sharp S–H bond state observed for the pristine MoS_2 materials, the H s-state overlap is more characteristic of H binding to flat transition metal surfaces.[64] Indeed, a very similar pattern is observed in the DOS for H adsorbing to a Pt(111) surface at either the fcc or top site (see Fig. S10 and S11 in the ESI†). Therefore, it is suggested that H adsorption on Mo at the S-vacancy defect may be governed by similar factors to H adsorption on transition metal surfaces.

Another interesting feature in the DOS arises when H adsorbs to the flat basal plane or the nanotube S-vacancy sites – a sharp partially occupied state with S p and Mo d character appears at the Fermi level. In the case of H adsorbing to transition metal surfaces (*e.g.* Pt(111) in Fig. S9 the ESI†) this state is not visible, perhaps due to the conducting nature of the surface which has states already spanning the Fermi level. It is possible this state is evidence of electron transfer from Mo to H as a bond forms. Indeed, Bader charge analyses of the flat and nanotube surfaces indicate that H gains negative charge density

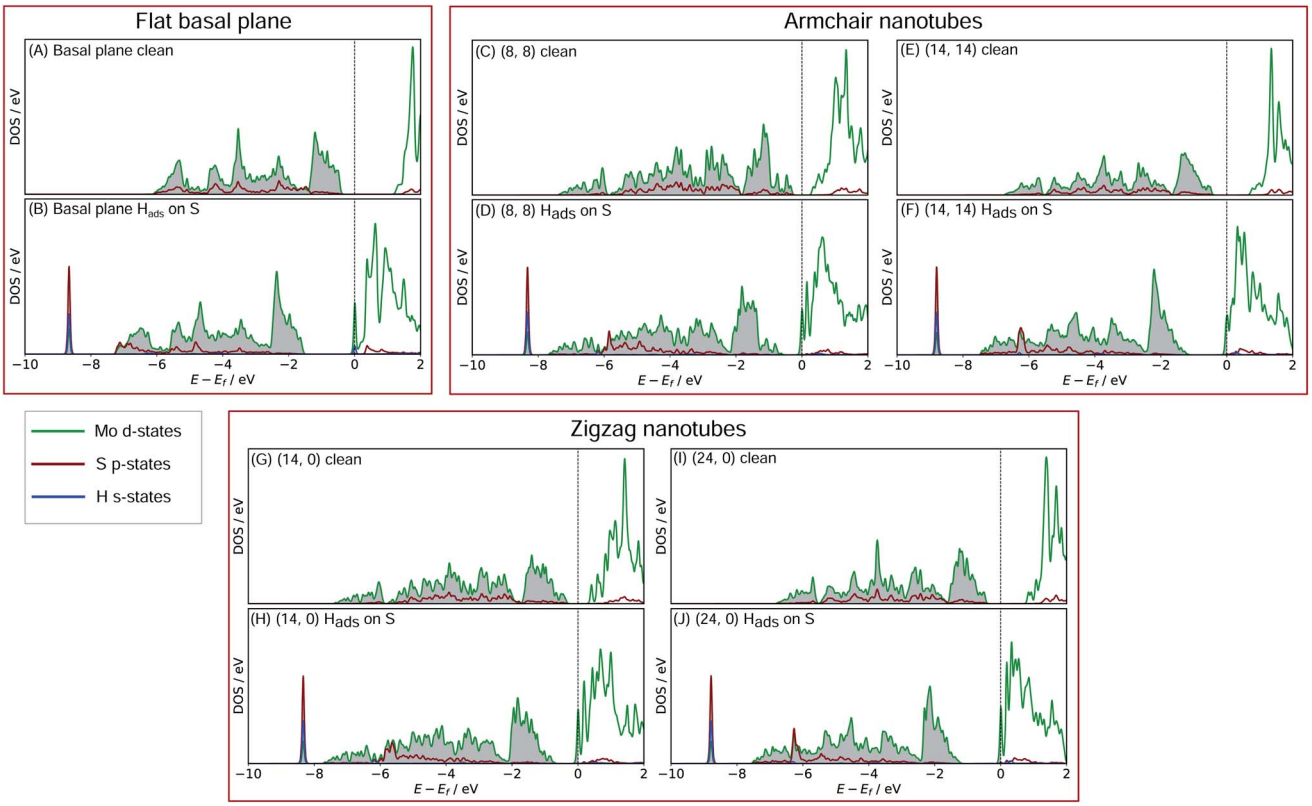

Fig. 6 Density of states (DOS) plots for the MoS_2 basal plane either (A) clean or (B) with H_{ads} on S. Plots (C) through to (F) show the same cases for (8, 8) and (14, 14) nanotubes, which are the two size extremes of the armchair nanotubes studied here. Plots (G) through (J) show this for the (14, 0) and (24, 0) zigzag nanotubes, again on the edges of the size range explored here. In all cases, the H s-state density is taken from the single adsorbed H, the S p-state density is from the S adsorption site, and the Mo d-state density is from all three directly neighbouring Mo atoms.

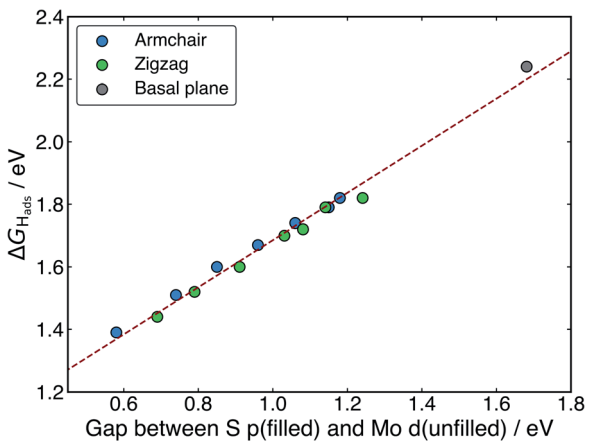

Fig. 7 The linear relation between $\Delta G_{H_{ads}}$ at an S atom and the energy gap between the filled S p-states of the adsorption site and the unfilled Mo d-states of neighbouring atoms. The data from armchair and zigzag nanotubes of different sizes are plotted here, and the flat basal plane is also shown to fit on the same trend.

on adsorbing ($0.4e^-$ equivalents), and the Mo atoms it binds to also lose about $0.3e^-$ equivalents together.

With H binding to Mo atoms at the S-vacancy defect on the flat basal plane,[30] it has been previously found that the adsorption can be understood using d-band theory,[65] which is typically applied to understand adsorption to pure metal surfaces. This model suggests that the binding strength of H will be proportional to the energy gap between the H s-states (set to 0 eV) and the Mo d-states, with a smaller gap meaning stronger binding. Application of this model to the S-vacancy is rational when considering the DOS analyses indicate that the H adsorption character is very similar to that on flat transition metals, as discussed above. Ouyang *et al.*[30] have previously found that there is no relation between $\Delta G_{H_{ads}}$ and the *centre* of the Mo d-band in flat MoS_2, as it is only the states close to the Fermi level that are involved in adsorbing H. It makes more sense to only consider these high energy d-states because, in contrast to the pure transition metals, the d-orbitals in the S-vacancy site are inequivalent. In the present work we affirm this for MoS_2 nanotubes. If $\Delta G_{H_{ads}}$ is plotted against the d-band centre for both armchair and zigzag nanotubes, no clear relation is seen (Fig. S10 in the ESI†). Instead, when plotting the edge of the Mo d-band against $\Delta G_{H_{ads}}$ (Fig. 9), an interesting pattern is observed. A linear relation exists, yet this relation appears to have a different slope for the armchair and zigzag nanotubes.

Returning to the d-band model,[65] the slope of the relation between $\Delta G_{H_{ads}}$ and the d-state edge would be determined by the amount of overlap between the H atom states and the Mo states (*i.e.* the coupling matrix). For armchair nanotubes, H binds between two Mo atoms that are closer together than on the

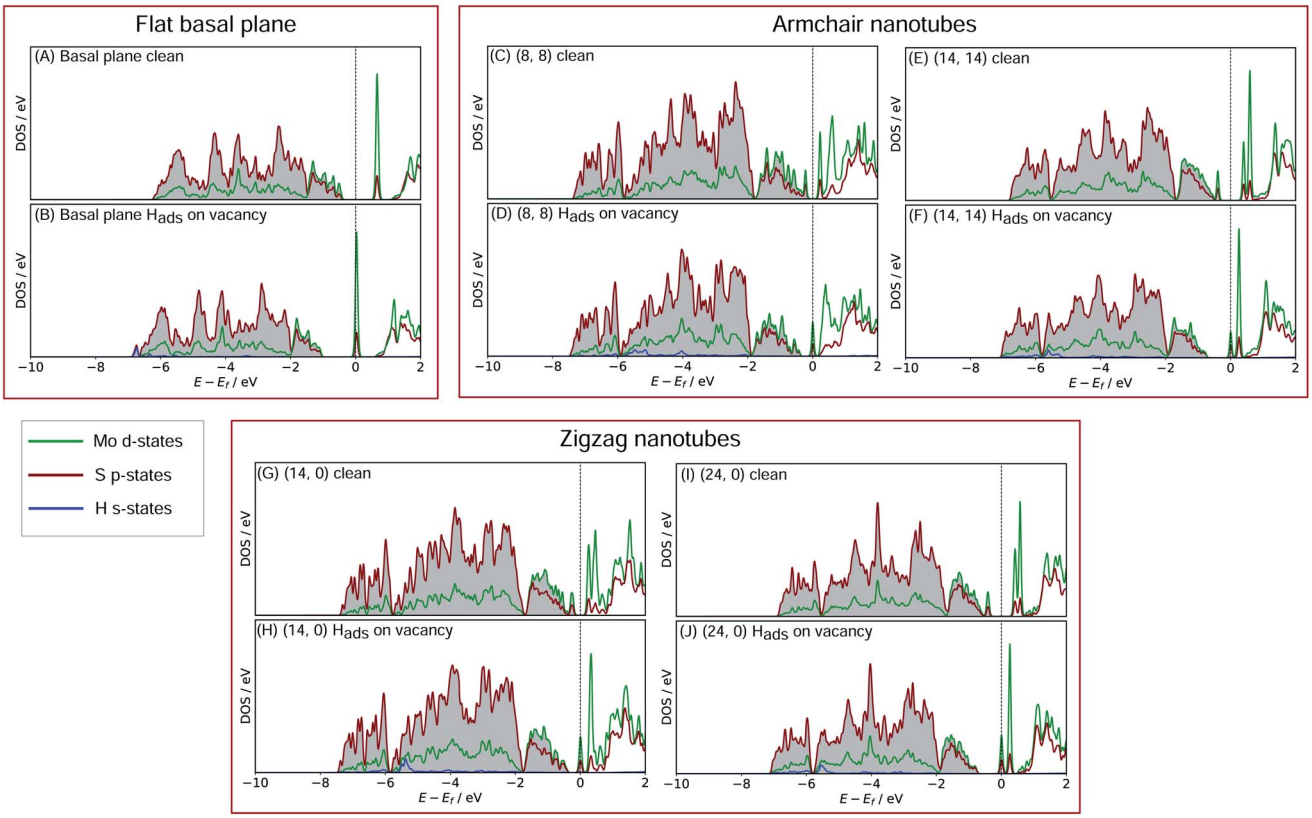

Fig. 8 Density of states (DOS) plots for the defective S-vacancy MoS_2 basal plane either (A) clean or (B) with H_{ads} at the vacancy site. Plots (C) through to (F) show the same cases for (8, 8) and (14, 14) nanotubes, which are the two size extremes of the armchair nanotubes studied here. Plots (G) through (J) show this for the (14, 0) and (24, 0) zigzag nanotubes, again on the edges of the size range explored here. In all cases, the H s-state density is taken from the single adsorbed H, the Mo d-state density is from the Mo atoms directly where H adsorbs (three atoms for the flat surface, and two for the nanotubes), and the S p-state density is from all neighbouring S atoms.

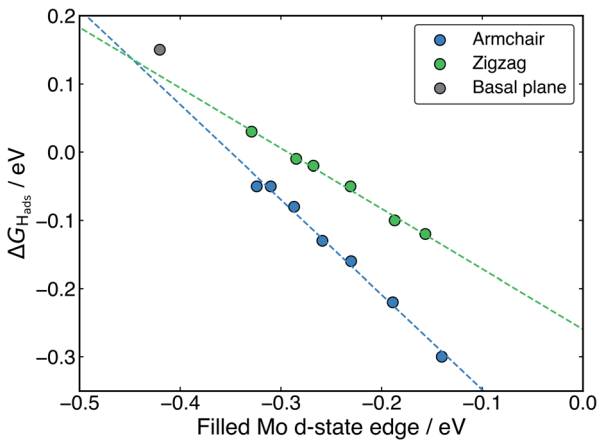

Fig. 9 The relation between the Mo d-state edge and the H adsorption free energy at S-vacancy defect site across different MoS_2 nanotubes and the flat basal plane. Note that two linear relations of different slope describe the armchair and zigzag nanotubes respectively.

zigzag nanotube (as outlined in a previous section). This would suggest a larger coupling matrix for H adsorbing on the armchair nanotube, which is likely what gives rise to the steeper slope for the armchair nanotubes in Fig. 9. The flat basal plane lies somewhat offset from the line described by either form of nanotube, indicating the coupling matrix may be once again different in this case.

Overall, the existence of this trend suggests that the d-band model can be accurately applied to H adsorption at MoS_2 S-vacancy sites, provided one uses only the Mo d-states that are involved in bonding (*i.e.* the highest energy states, represented by the edge of the d-band). The change in the d-band edge that generates this effect on $\Delta G_{H_{ads}}$ is also shown plotted as a function of nanotube diameter in Fig. S11 in the ESI.† Indeed, the relation in Fig. 9 suggests that ideal HER thermodynamics ($\Delta G_{H_{ads}} = 0$) arise for MoS_2 materials with d-band edges between −0.4 and −0.3 eV below the Fermi level. However, this depends on the specific structure of the Mo atoms in S-vacancy defect, which determines the coupling matrix. Going forwards, it may also be interesting to examine charge polarisation on the Mo centres in defect sites. This metric has previously been used to explain N adsorption trends on transition metal single-atom catalysts supported by boron carbide nanotubes.[66]

4 Conclusions

This work represents the first computational study of hydrogen evolution on MoS_2 nanotubes. Density functional theory is used

to systematically examine the H adsorption energies for pristine armchair and zigzag nanotubes, as well as nanotubes with an S-vacancy, across a range of different diameters. For the pristine nanotubes, there is a strong preference for H to adsorb on the outside as opposed to the inside of the nanotube, with the favourable adsorption site being directly on-top of an S atom. We also observe a relationship between the nanotube diameter and the H adsorption free energy ($\Delta G_{H_{ads}}$), such that smaller and more strained tubes adsorb H stronger. $\Delta G_{H_{ads}}$ ranges between 1.82 and 1.39 eV as the nanotube diameter decreases from 22 to 12 Å. From density of states calculations across the different sized nanotubes, a very reliable linear relation is found between $\Delta G_{H_{ads}}$ and the energy gap between the filled S p-states and the unfilled Mo d-states. These two states are implicated in electron transfer when H adsorbs, and thus we propose this energy gap – which is seen to close as the nanotubes get smaller – is determining the H adsorption energy.

For the S-vacancy sites on the MoS_2 nanotubes, H adsorbs significantly stronger than on the pristine nanotubes with $\Delta G_{H_{ads}}$ in the range of 0.03 to −0.30 eV, depending on the nanotube diameter. For zigzag nanotubes at around 20 Å in diameter, the $\Delta G_{H_{ads}}$ values are exactly at the 0 eV mark, which is thermodynamically ideal for hydrogen evolution. Given S-vacancy defects are common in MoS_2 nanotubes,[28,29] this suggests tubes of approximately this diameter would be highly promising hydrogen evolution catalysts. From density of states calculations, it is seen that the binding of H at the defect resembles adsorption to metallic surfaces, and is dissimilar to the distinct S–H covalent bond observed for the pristine nanotubes. Additionally, the variation in $\Delta G_{H_{ads}}$ appears to be governed by different factors. The trend in $\Delta G_{H_{ads}}$ when H binds to Mo atoms at the defect site is rationalised using the classic d-band model for adsorption on metals.[65] A strong linear relation is observed between the position of the d-states in Mo and $\Delta G_{H_{ads}}$, which differs for armchair and zigzag nanotubes due to different coupling matrices in the Mo–H bond.

Overall, these findings suggest that MoS_2 nanotubes are highly promising for hydrogen evolution, and that their activity may be readily modified by controlling the size distribution of the tubes. Additionally, the electronic explanations of the factors affecting H adsorption that we report here can be used to assist in the rational improvement of current MoS_2 catalysts, or aid in the design of novel hydrogen evolution catalysts.

Conflicts of interest

There are no conflicts to declare.

Acknowledgements

The authors acknowledge financial support from the MacDiarmid Institute for Advanced Materials and Nanotechnology and the University of Otago. Special thanks also go to the New Zealand eScience Infrastructure (NeSI), funded through the New Zealand Ministry of Business, Innovation and Employment. NeSI's high performance computing facilities allowed this work to be performed.

Notes and references

1 J. O. Bockris and E. C. Potter, *J. Electrochem. Soc.*, 1952, **99**, 169.
2 G. Glenk and S. Reichelstein, *Nat. Energy*, 2019, **4**, 216–222.
3 A. M. Abdalla, S. Hossain, O. B. Nisfindy, A. T. Azad, M. Dawood and A. K. Azad, *Energy Convers. Manag.*, 2018, **165**, 602–627.
4 J. Brightling, *Johnson Matthey Technol. Rev.*, 2018, **62**, 32–47.
5 I. Dincer and C. Acar, *Int. J. Hydrogen Energy*, 2014, **40**, 11094–11111.
6 N. Z. Muradov and T. N. Veziroğlu, *Int. J. Hydrogen Energy*, 2005, **30**, 225–237.
7 M. S. Dresselhaus and I. L. Thomas, *Nature*, 2001, **414**, 332–337.
8 E. Skúlason, G. S. Karlberg, J. Rossmeisl, T. Bligaard, J. Greeley, H. Jónsson and J. K. Nørskov, *Phys. Chem. Chem. Phys.*, 2007, **9**, 3241–3250.
9 E. Skúlason, V. Tripkovic, M. E. Bjorketun, S. Gudmundsdottir, G. Karlberg, J. Rossmeisl, T. Bligaard, H. Jónsson and J. K. Nørskov, *J. Phys. Chem. C*, 2010, **114**, 18182–18197.
10 J. Greeley, T. Jaramillo, J. Bonde, I. Chorkendorff and J. K. Nørskov, *Nat. Mater.*, 2006, **5**, 909–913.
11 T. F. Jaramillo, K. P. Jørgensen, J. Bonde, J. H. Nielsen, S. Horch and I. Chorkendorff, *Science*, 2007, **317**, 100–102.
12 J. Bonde, P. G. Moses, T. F. Jaramillo, J. K. Nørskov and I. Chorkendorff, *Faraday Discuss.*, 2009, **140**, 219–231.
13 J. D. Benck, T. R. Hellstern, J. Kibsgaard, P. Chakthranont and T. F. Jaramillo, *ACS Catal.*, 2014, **4**, 3957–3971.
14 B. Hinnemann, P. G. Moses, J. Bonde, K. P. Jørgensen, J. H. Nielsen, S. Horch, I. Chorkendorff and J. K. Nørskov, *J. Am. Chem. Soc.*, 2005, **127**, 5308–5309.
15 C. Tsai, K. Chan, J. K. Nørskov and F. Abild-Pedersen, *Surf. Sci.*, 2015, **640**, 133–140.
16 C. Tsai, F. Abild-Pedersen and J. K. Nørskov, *Nano Lett.*, 2014, **14**, 1381–1387.
17 J. K. Nørskov, T. Bligaard, A. Logadottir, J. R. Kitchin, J. G. Chen, S. Pandelov and U. Stimming, *J. Electrochem. Soc.*, 2005, **152**, 23–26.
18 J. Kibsgaard, A. Tuxen, K. G. Knudsen, M. Brorson, H. Topsøe, E. Lægsgaard, J. V. Lauritsen and F. Besenbacher, *J. Catal.*, 2010, **272**, 195–203.
19 D. Escalera-López, Y. Niu, J. Yin, K. Cooke, N. V. Rees and R. E. Palmer, *ACS Catal.*, 2016, **6**, 6008–6017.
20 Y. Li, H. Wang, L. Xie, Y. Liang, G. Hong and H. Dai, *J. Am. Chem. Soc.*, 2011, **133**, 7296–7299.
21 C. Ruffman, C. K. Gordon, J. T. Gilmour, F. D. Mackenzie and A. L. Garden, *Nanoscale*, 2021, **13**, 3106–3118.
22 S. Trasatti, *J. Electroanal. Chem.*, 1972, **39**, 163–184.
23 S. Tang, W. Wu, S. Zhang, D. Ye, P. Zhong, X. Li, L. Liu and Y. F. Li, *Phys. Chem. Chem. Phys.*, 2018, **20**, 1861–1871.
24 Y. Shi, Y. Zhou, D. R. Yang, W. X. Xu, C. Wang, F. B. Wang, J. J. Xu, X. H. Xia and H. Y. Chen, *J. Am. Chem. Soc.*, 2017, **139**, 15479–15485.

25 S. Park, J. Park, H. Abroshan, L. Zhang, J. K. Kim, J. Zhang, J. Guo, S. Siahrostami and X. Zheng, *ACS Energy Lett.*, 2018, **3**, 2685–2693.
26 C. Tsai, H. Li, S. Park, J. Park, H. S. Han, J. K. Nørskov, X. Zheng and F. Abild-Pedersen, *Nat. Commun.*, 2017, **8**, 1–8.
27 G. Gao, Q. Sun and A. Du, *J. Phys. Chem. C*, 2016, **120**, 16761–16766.
28 W. Zhou, X. Zou, S. Najmaei, Z. Liu, Y. Shi, J. Kong, J. Lou, P. M. Ajayan, B. I. Yakobson and J. C. Idrobo, *Nano Lett.*, 2013, **13**, 2615–2622.
29 H. Qiu, T. Xu, Z. Wang, W. Ren, H. Nan, Z. Ni, Q. Chen, S. Yuan, F. Miao, F. Song, G. Long, Y. Shi, L. Sun, J. Wang and X. Wang, *Nat. Commun.*, 2013, **4**, 1–6.
30 Y. Ouyang, C. Ling, Q. Chen, Z. Wang, L. Shi and J. Wang, *Chem. Mater.*, 2016, **28**, 4390–4396.
31 H. Li, C. Tsai, A. L. Koh, L. Cai, A. W. Contryman, A. H. Fragapane, J. Zhao, H. S. Han, H. C. Manoharan, F. Abild-Pedersen, J. K. Nørskov and X. Zheng, *Nat. Mater.*, 2016, **15**, 48–53.
32 M. A. Lukowski, A. S. Daniel, F. Meng, A. Forticaux, L. Li and S. Jin, *J. Am. Chem. Soc.*, 2013, **135**, 10274–10277.
33 D. Voiry, M. Salehi, R. Silva, T. Fujita, M. Chen, T. Asefa, V. B. Shenoy, G. Eda and M. Chhowalla, *Nano Lett.*, 2013, **13**, 6222–6227.
34 L. Song, M. Zhao, X. Li, Z. Zhang and L. Qu, *RSC Adv.*, 2016, **6**, 70740–70746.
35 X. Zhou, J. Prikryl, M. Krbal, J. M. Macak and P. Schmuki, *Electrochem. Commun.*, 2017, **82**, 112–116.
36 W. Jian, X. Cheng, Y. Huang, Y. You, R. Zhou, T. Sun and J. Xu, *Chem. Eng. J.*, 2017, **328**, 474–483.
37 M. Remskar, A. Mrzel, Z. Skraba, A. Jesih, M. Ceh, J. Demšar, P. Stadelmann, F. Lévy and D. Mihailovic, *Science*, 2001, **292**, 479–481.
38 F. L. Deepak and M. Jose-Yacaman, *Isr. J. Chem.*, 2010, **50**, 426–438.
39 W. Shi, Z. Wang and Y. Q. Fu, *J. Nanoparticle Res.*, 2017, **19**, 1–7.
40 R. de Alencar Rocha, W. F. da Cunha and L. A. Ribeiro, *J. Mol. Model.*, 2019, **25**, 290.
41 W. Li, G. Zhang, M. Guo and Y.-W. W. Zhang, *Nano Res.*, 2014, **7**, 1–10.
42 J. Xiao, M. Long, X. Li, H. Xu, H. Huang and Y. Gao, *Sci. Rep.*, 2014, **4**, 1–7.
43 G. L. Cardoso, P. C. Piquini and R. Ahuja, *Energy Fuels*, 2021, **21**, 40.
44 G. Seifert, H. Terrones, M. Terrones, G. Jungnickel and T. Frauenheim, *Phys. Rev. Lett.*, 2000, **85**, 146–149.
45 R. Ansari, S. Malakpour, M. Faghihnasiri and S. Sahmani, *Superlattices Microstruct.*, 2015, **82**, 188–200.
46 G. Kresse and J. Furthmüller, *Comput. Mater. Sci.*, 1996, **6**, 15–50.
47 J. Wellendorff, K. T. Lundgaard, A. Møgelhøj, V. Petzold, D. D. Landis, J. K. Nørskov, T. Bligaard and K. W. Jacobsen, *Phys. Rev. B: Condens. Matter Mater. Phys.*, 2012, **85**, 235149.
48 P. E. Blöchl, *Phys. Rev. B: Condens. Matter Mater. Phys.*, 1994, **50**, 17953–17979.
49 G. Kresse and D. Joubert, *Phys. Rev. B: Condens. Matter Mater. Phys.*, 1999, **59**, 1758.
50 S. Xiong and G. Cao, *Nanotechnology*, 2016, **27**, 105701.
51 H.-P. Komsa and A. V. Krasheninnikov, *Phys. Rev. B: Condens. Matter Mater. Phys.*, 2015, **91**, 125304.
52 R. Kronberg, M. Hakala, N. Holmberg and K. Laasonen, *Phys. Chem. Chem. Phys.*, 2017, **19**, 16231–16241.
53 L. Margulis, G. Salitra, R. Tenne, M. Talianker and M. Tallanker, *Nature*, 1993, **365**, 113–114.
54 M. Liu, M. S. Hybertsen and Q. Wu, *Angew. Chem.*, 2020, **132**, 2–9.
55 Y. Huang, R. J. Nielsen, W. A. Goddard III and M. P. Soriaga, *J. Am. Chem. Soc.*, 2015, **137**, 6692–6698.
56 C. Ruffman, C. K. Gordon, E. Skúlason and A. L. Garden, *J. Phys. Chem. C*, 2020, **124**, 17015–17026.
57 W. Li, G. Liu, J. Li, Y. Wang, L. Ricardez-Sandoval, Y. Zhang and Z. Zhang, *Appl. Surf. Sci.*, 2019, 143869.
58 T. Niyitanga, P. E. Evans, T. Ekanayake, P. A. Dowben and H. K. Jeong, *J. Electroanal. Chem.*, 2019, **845**, 39–47.
59 H. Wang, H. J. Lin, W. T. Cai, L. Z. Ouyang and M. Zhu, *J. Alloys Compd.*, 2016, **658**, 280–300.
60 Q. L. Xiong, J. Zhang, C. Xiao and Z. H. Li, *Phys. Chem. Chem. Phys.*, 2017, **19**, 19948–19958.
61 Y. Yang, Y. Liu, B. Man, M. Zhao and W. Li, *RSC Adv.*, 2019, **9**, 17203–17210.
62 E. Skúlason, A. A. Faraj, L. Kristinsdóttir, J. Hussain, A. L. Garden and H. Jónsson, *Top. Catal.*, 2014, **57**, 273–281.
63 K. Honkala, A. Hellman, I. N. Remediakis, A. Logadottir, A. Carlsson, S. Dahl, C. H. Christensen and J. K. Nørskov, *Science*, 2005, **307**, 555–558.
64 P. Légaré, *Surf. Sci.*, 2004, **559**, 169–178.
65 B. Hammer and J. K. Nørskov, *Surf. Sci.*, 1995, **343**, 211–220.
66 T. Liu, Q. Dang, X. Zhou, J. Li, Z. Ge, H. Che, S. Tang, Y. Luo and J. Jiang, *Chem.–Eur. J.*, 2021, **27**, 6945–6953.